

## Key Points:

- Environmental Fe concentrations control the formation and evolution of allophane in Al-Si-Fe systems
- Near-infrared spectra (1.2–2.6  $\mu\text{m}$ ) show incapability in identifying short-range ordered minerals in Al-Si-Fe systems
- Co-occurrence of allophane and akaganeite would constrain the local palaeoenvironment on Mars

## Supporting Information:

- Supporting Information S1

## Correspondence to:

P. Yuan,  
[yuanpeng@gig.ac.cn](mailto:yuanpeng@gig.ac.cn)






## Citation:

Du, P., Yuan, P., Liu, J., Yang, Y., Bu, H., Wang, S., et al. (2020). Effects of environmental Fe concentrations on formation and evolution of allophane in Al-Si-Fe systems: Implications for both Earth and Mars. *Journal of Geophysical Research: Planets*, 125, e2020JE006590. <https://doi.org/10.1029/2020JE006590>

Received 22 JUN 2020

Accepted 3 NOV 2020

## Effects of Environmental Fe Concentrations on Formation and Evolution of Allophane in Al-Si-Fe Systems: Implications for Both Earth and Mars

Peixin Du<sup>1</sup> , Peng Yuan<sup>1,2</sup> , Jiacheng Liu<sup>3</sup>, Yixuan Yang<sup>1,2</sup>, Hongling Bu<sup>4</sup>, Shun Wang<sup>1,2</sup> , Junming Zhou<sup>1,2</sup>, Hongzhe Song<sup>1,2</sup>, Dong Liu<sup>1,2</sup>, Joseph R. Michalski<sup>3</sup> , and Chengshuai Liu<sup>4</sup> 

<sup>1</sup>CAS Key Laboratory of Mineralogy and Metallogeny/Guangdong Provincial Key Laboratory of Mineral Physics and Materials, Guangzhou Institute of Geochemistry, Chinese Academy of Sciences, Guangzhou, China, <sup>2</sup>University of Chinese Academy of Sciences, Beijing, China, <sup>3</sup>Department of Earth Sciences, The University of Hong Kong, Hong Kong, China, <sup>4</sup>Guangdong Key Laboratory of Integrated Agro-environmental Pollution Control and Management, Guangdong Institute of Eco-environmental Science & Technology, Guangdong Academy of Sciences, Guangzhou, China

**Abstract** Allophane, a common component on Earth and a probable constituent of the amorphous component on Mars, is closely associated with Fe in the form of structural Fe and/or iron (oxyhydr)oxide coatings. However, until now, the formation and evolution of allophane as products of environmental Fe concentrations have rarely been studied. We investigated allophane precipitation from gels with different Fe/(Fe + Al) molar ratios ( $n$ ,  $0 \leq n \leq 1.0$ ). X-ray diffraction patterns and Fourier transform infrared spectra of the products showed that allophane was nearly the only product at  $n \leq 0.2$  and that the crystallinity of Fe-rich allophane decreased with increasing  $n$ . Combined with the results of transmission electron microscopy and Mössbauer spectroscopy, Fe was found to be mainly incorporated into the gibbsite-like sheet of allophane, forming clusters; the highest Fe-for-Al substitution content was roughly estimated to be 20 mol.%. As  $n$  increased further, the formation of allophane was increasingly suppressed, and the Fe phases began to separate from the Al-Si phases, resulting in mixtures of incipient allophane and incipient akaganeite and finally akaganeite. The near-infrared spectroscopic data (1.2–2.6  $\mu\text{m}$ ) of the products showed incapability in identifying poorly ordered minerals in Al-Si-Fe systems, while the features in the range of 0.4–1.2  $\mu\text{m}$  were powerful for studying iron occurrence in the products. These findings not only offer insights into the formation, evolution and geological role of allophane in Al-Si-Fe systems on Earth but also help constrain the paleoenvironment of locations where allophane and akaganeite co-occur on Mars.

### 1. Introduction

Identifying the mineralogy on the surface of Mars helps to deduce the formation and evolution of sediments and the possible paleoenvironments involved (e.g., Bishop et al., 2018; Fraeman et al., 2013). At present, based on the visible and near-infrared (VNIR) spectroscopic data collected by the Compact Reconnaissance Imaging Spectrometer for Mars (CRISM) onboard the Mars Reconnaissance Orbiter and Observatoire pour la Minéralogie, l'Eau, les Glaces et l'Activité (OMEGA) onboard the Mars Express orbiter, the global mineralogy on Mars, including mainly the distribution of phyllosilicate (Poulet et al., 2005) and hydrated sulfates (Gendrin et al., 2005), has been recorded. Analyses of these data suggest that distinct aqueous geochemical environments existed on Mars, including warm surface waters (Bishop & Rampe, 2016), subsurface hydrothermal systems (Ehlmann et al., 2011) and hot springs (Al-Samir et al., 2017). For instance, the phyllosilicate outcrops on the surface of Mars mainly include Fe-Mg smectite (Ehlmann & Edwards, 2014); on the basis of the fact that smectite minerals typically occurs in surficial soils or sediments on Earth (Chamley, 1989), these outcrops might have formed in warm waters (25°C–50°C) on early Mars.

Apart from the above mentioned well-crystallized minerals, data from both orbital spectroscopy and in situ rover investigations suggest the wide distribution of poorly crystallized and amorphous hydrated minerals on the surface of Mars, such as opal-A, allophane, and ferrihydrite (e.g., Rampe et al., 2012; Vaniman et al., 2014). Among them, allophane and allophane-like materials are considered to be common

components of the Martian surface. Based on mass balance calculations, Ming et al. (2006) suggested that allophane might be present in the weathering rocks at Gusev Crater. Later, allophane-like materials were widely identified in several low-albedo regions of Mars with the aid of thermal emission spectroscopy (Rampe et al., 2012); their contents in sediments reach 28% in Northern Acidalia and are higher than 10% in other low-albedo areas. Amorphous phases that might contain allophane have been detected at Rocknest by the instruments on Curiosity rover (Blake et al., 2013). Moreover, allophane-like materials have been identified at Mawrth Vallis based on the analysis of the CRISM data (Bishop & Rampe, 2016).

Due to their metastable nature in the presence of water and high sensitivity to environmental changes, allophane-like materials carry more geological significance than well-crystallized minerals; they can provide key constraints on localized geochemical settings and help to refine the geological evolution of Mars (Bishop & Rampe, 2016). Whereas, allophane on Earth is mainly formed by the low-temperature hydration of volcanic glass under weakly acidic to neutral environments ( $\text{pH} = 5\text{--}7$ ) (Colman, 1982; Wada, 1989), the presence of allophane-rich regions on Mars indicates that weakly acidic to neutral chemical weathering occurred locally on Mars, in contrast with previous models that suggested the occurrence of global-scale strongly acidic weathering on Mars (Rampe et al., 2012). The occurrence of allophane also indicates that the climate changes in these regions are quick and therefore unable to provide the conditions necessary for crystallized clay minerals to form, that is, a warm climate and long retention of surface water (Bishop et al., 2018).

Weitz et al. (2014) discovered relatively fresh exposures of hydrated, amorphous Al-Si-Fe gels along the wall rock slopes in Coprates Chasma, Mars, and identified them as Fe-rich allophane by analyzing the VNIR spectroscopic data collected by CRISM; the VNIR bands of Fe-rich allophane are wider and shift to the larger-wavenumber side compared to those of Fe-free allophane. The occurrence of Fe-rich allophane provides additional information about the history of water and aqueous alteration on Mars (Weitz et al., 2014), including the following: (i) apart from large amounts of Al and Si, a certain amount of Fe also exists in this sediment environment; and (ii) the Fe-rich allophane in these deposits may eventually recrystallize into Fe-bearing clay minerals such as nontronite (Farmer et al., 1991), while Fe-free allophane may transform into montmorillonite, halloysite or gibbsite (Bishop & Rampe, 2016; Colman, 1982). The identification of Fe-rich allophane and the deduction of the related paleoenvironment are based on the comparative analysis of the spectral features of sediments on Mars detected by orbiters with those of the corresponding minerals on Earth and on the understanding of the way in which iron occurrence in allophane affects its spectral features.

Allophane is a hydrous aluminosilicate mineraloid ubiquitously distributed in supergene weathering environments, such as soils altered from tephra and leached layers of weathering crusts (Levard & Basile-Doelsch, 2016). It appears as an aggregate of hollow nanospheres with a chemical formula of  $1\text{--}2\text{SiO}_2\cdot\text{Al}_2\text{O}_3\cdot 5\text{--}6\text{H}_2\text{O}$  (Du et al., 2018). Its isolated particle has an external diameter of 3.5–5 nm and a wall thickness of 0.7–1.0 nm. Several openings with a diameter of approximately 0.3–0.5 nm exist in the wall, which serve as passages for small molecules such as  $\text{H}_2\text{O}$  (Wada, 1989; Wang et al., 2018). Curved gibbsite-like sheets, of which the interior Al–OH is substituted by orthosilicic groups ( $\text{O}_3\text{SiOH}$ ), constitute the skeleton of allophane, with the excess Si attached to the interior of the skeleton in the form of oligomers (Du et al., 2020). Allophane is formed, in most cases, by the coprecipitation of  $\text{Al}_2\text{O}_3$  and  $\text{SiO}_2$  sols followed by weak crystallization under certain conditions (Wada, 1987). In the typical genesis environments of allophane, where fast chemical weathering of volcanic materials is driven by high rainfall and low pH, Al, Si, and Fe always exist as inorganic ions or sols (Harsh, 2012), providing the basis for Fe atoms to be incorporated into the allophane structure. Additionally, natural allophane often co-occurs with iron (oxyhydr)oxides such as ferrihydrite (Parfitt et al., 1988). Therefore, Fe is considered to be closely associated with natural allophane in the form of structural Fe and/or iron (oxyhydr)oxide coatings.

Since the 1970s, studies have shown that for natural allophane, of which the free Fe is removed by selective chemical dissolution, a certain amount of Fe can still be detected, which has been attributed to the structural Fe (e.g., Horikawa & Soezima, 1977; Kitagawa, 1973). However, the structure of allophane was not clearly known at that time, not to mention the occurrence of Fe in the allophane structure. Studies in recent years have suggested the existence of Fe-rich allophane in soils and sediments (e.g., Filimonova et al., 2016; Kaufhold et al., 2009) but did not provide any direct evidence for the presence of the structural Fe. To date,

regarding Fe-rich allophane, only Baker and co-workers synthesized Fe-rich allophane (with ~1 mol.% Al substituted by Fe) by a hydrothermal method (Baker et al., 2014; Weitz et al., 2014).

From the above, even for Earth's allophane, the effects of environmental Fe concentrations on allophane formation in the Al-Si-Fe system and the effects of Fe occurrence in allophane on its spectral features are ambiguous, which hinders not only the understanding of allophane's formation, evolution and even its geochemical role in the supergene weathering environments on Earth but also the identification of poorly ordered minerals and deduction of the involved paleoenvironment on Mars. To this end, the objectives of this study are as follows: (i) to reveal the effects of environmental Fe concentrations on the formation and evolution of allophane in Al-Si-Fe systems; and (ii) to study the effects of Fe occurrence in allophane on its spectral features. To achieve the above goals, various amounts of Fe (III) are introduced into the hydrothermal synthesis system of allophane. A combination of techniques, including X-ray diffraction (XRD), Fourier transform infrared (FTIR) spectroscopy, transmission electron microscopy (TEM) and Mössbauer spectroscopy, are used to detect changes in the structure and phases of the products induced by Fe introduction. VNIR spectroscopy is used to further characterize the changes in the spectral features of the products for possible comparative studies on Mars.

## 2. Experimental

### 2.1. Materials and Methods

The procedure for synthesizing Fe-rich allophane was a modified version of that described by Montarges-Pelletier et al. (2005). All chemicals and reagents used in this study were of analytical grade and used as received. Ultrapure water with a resistivity of 18.25 M $\Omega$ -cm was used throughout the experiments. The precursors were prepared by adding defined amounts of tetraethylorthosilicate (TEOS, Aldrich, USA) to 225 mL of 0.10 M chloride solutions (AlCl<sub>3</sub> and FeCl<sub>3</sub>, Aladdin, China) to an initial Si/(Al + Fe) molar ratio of 0.75 and initial Fe/(Al + Fe) molar ratios ( $n$ ) of 0, 0.01, 0.02, 0.05, 0.1, 0.2, 0.3, 0.5, 0.7, 0.9, and 1.0 under stirring. Then, 225 mL of 0.2 M NaOH was added into each dispersion at a rate of 1.0 mL/min, after which the dispersions were stirred for another hour to ensure the complete hydrolysis of the TEOS. Note here that a high H<sub>2</sub>O/Si molar ratio led to an almost complete conversion of TEOS to Si(OH)<sub>4</sub> prior to the occurrence of significant condensation (Doelsch et al., 2000). The dispersions were aged at room temperature overnight and then autoclaved at 100°C for 48 h. Then, a portion of each dispersion was withdrawn for microscopic characterizations, and the remainder was coagulated by adding diluted ammonia to a pH of ~7.0 and centrifuged at 11,000 rpm for 5 min to remove byproducts such as NaCl. The resulting gels were dialyzed (3,000 Da) in ultrapure water for 4 days and freeze-dried. The obtained powders were labeled  $Fe_n$  (e.g., Fe0, Fe0.01, Fe0.02, and so on). For example, Fe0.01 was the product obtained at  $n = 0.01$ .

### 2.2. Characterization Techniques

XRD analysis was performed on a Rigaku D/max-1200 diffractometer (Rigaku, Japan) with Co K $\alpha$  radiation ( $\lambda = 1.78899$  Å) generated at 40 kV and 15 mA. The specimens were investigated from 5° to 80° (2 $\theta$ ) with a step size of 0.02° and a measuring time of 1.0 s per step.

FTIR spectra were recorded in a transmission mode using a Bruker Vertex 70 IR spectrometer (Manheim, Germany) at room temperature. The specimens were prepared by mixing 0.9 mg of sample and 80 mg of KBr followed by pressing the mixtures into pellets. The mixtures and pellets were placed under an infrared lamp to minimize the amounts of physisorbed water before measurements were taken. A pure KBr wafer was measured and used as the background. All of the spectra were collected over 64 scans in the range of 4,000–400 cm<sup>-1</sup> at a resolution of 4 cm<sup>-1</sup>.

TEM images (both bright and dark field images) were collected on an FEI Talos F200S field-emission transmission electron microscope operating at an accelerating voltage of 200 kV. To avoid the irreversible aggregation of allophane particles caused by capillary stress during drying (Du et al., 2020), the withdrawn dispersions were diluted into ethanol ultrasonically, and the specimens were prepared by dropping one droplet of the as-received dispersion onto a carbon-coated copper microgrid.

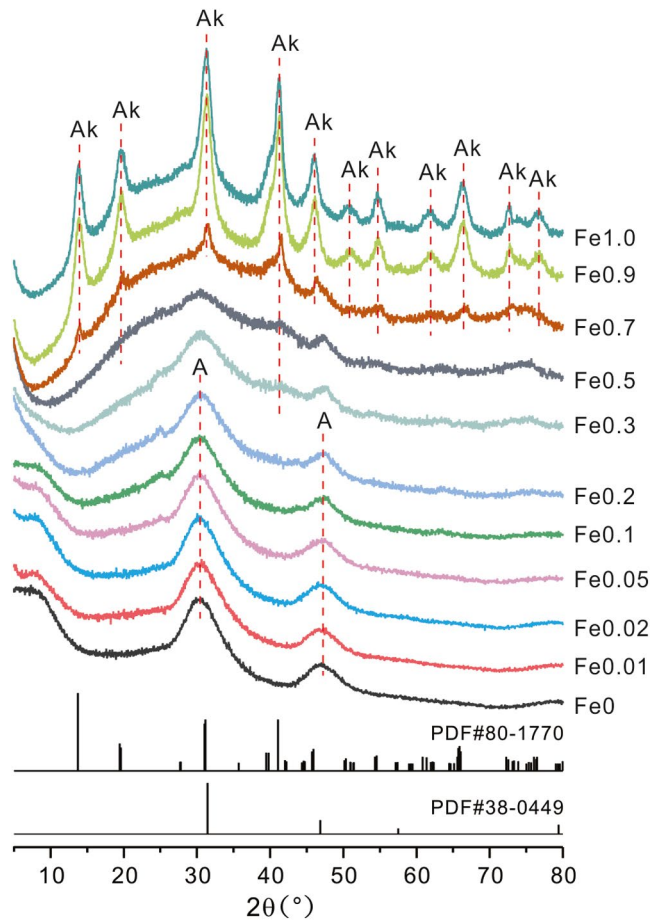


**Figure 1.** XRD patterns (CoK $\alpha$ ) of the products obtained at different initial Fe/(Fe + Al) molar ratios. A, allophane; Ak, akaganeite; XRD, X-ray diffraction.

Room-temperature and low-temperature (12 K)  $^{57}\text{Fe}$  Mössbauer spectra were recorded in transmission mode using a silver double limited WSS-10 Mössbauer spectrometer (WissEL GmbH, Germany) equipped with a Janis model SHE-850 closed cycle cryostat. All spectra were calibrated against a  $7\ \mu\text{m}$   $\alpha\text{-Fe}$  foil at room temperature (Barrero et al., 2006). The Mössbauer parameters, including isomer shift (IS), quadrupole splitting, hyperfine splitting field ( $B_{\text{hf}}$ ) and relative area, were obtained with a least-square fitting procedure using the MossWinn program with a Lorentzian line shape.

VNIR spectra were recorded using an ASD FieldSpec three reflectance spectrometer (Analytical Spectral Devices Inc., Colorado) that measures reflectance from 0.35 to  $2.5\ \mu\text{m}$ . A white reflectance standard Spectralon plate (Labsphere Inc., UK) was measured as a reference. The wavelength scanning interval was 1.4 nm in the range of 0.35– $1.0\ \mu\text{m}$  and 2 nm in the range of 1.0– $2.5\ \mu\text{m}$ , while the resolution ranged from 3 to 10 nm. 30 scans were averaged to improve the signal-to-noise ratio.

### 3. Results

#### 3.1. XRD Results

The changes in the structure and phases of the products were characterized by XRD, the results of which are shown in Figure 1. The background was not deducted in these plots to show the changes in any amorphous or poorly ordered phases in an appreciable amount. As exhibited in the XRD pattern of Fe0, two broad reflections at  $3.4\ \text{\AA}$  and  $2.2\ \text{\AA}$  appeared, which were consistent with those of natural allophane (Wada, 1989) and could be indexed to allophane (PDF#38-0449), indicating that allophane was the only product in the absence of Fe. At  $n \leq 0.2$ , the overall XRD patterns exhibited limited noticeable changes but slight decreases in reflection intensity and the reflection at  $3.4\ \text{\AA}$  seemed to broaden a bit, both indicating that the structural order of allophane slightly decreased with the presence of a minor amount of Fe. In these scenarios, Fe was believed to mainly substitute for Al in the allophane structure rather than form

associated iron (oxyhydr)oxides, albeit the presence of akaganeite has been shown by the following Mössbauer results.

At  $n = 0.3\text{--}0.5$ , the XRD patterns exhibited less-defined reflections at  $3.4\ \text{\AA}$  and  $2.2\ \text{\AA}$ , indicating that the formation of allophane was partly suppressed. Reflections at  $5.2\ \text{\AA}$  and  $2.5\ \text{\AA}$  began to appear, which might have arisen from the (002) and ( $-112$ ) planes of akaganeite (PDF#80-1770), a ferric oxyhydroxide mineral that includes, in its structure,  $0.5\ \text{nm}^2$  tunnels occupied by  $\text{Cl}^-$  (Cornell & Schwertmann, 2003). The poor discernibility of these two reflections suggests the incipient nature of the akaganeite. Overall, Fe-containing allophane or allophane-like materials dominated Fe0.3 but occurred only in a small amount in Fe0.5. Further crystallization and growth of the akaganeite occurred at higher  $n$  values. In Fe0.7, all of the reflections were indexed to akaganeite, suggesting the dominance of akaganeite. The broad reflections of the akaganeite were indicative of its small crystals (Schwertmann & Cornell, 1991) and/or of its poor structural order. For example, using Scherrer equation (Holzwarth & Gibson, 2011), the crystallite size in the direction perpendicular to ( $-101$ ) is calculated to be 16.8 nm. The very high background suggested the presence of a large number of amorphous materials. The center of the amorphous background seems to overlap with the (301) and ( $-103$ ) reflections of akaganeite and is located at  $\sim 3.3\ \text{\AA}$ , being adjacent to the characteristic reflection of silica-X (PDF#16-0380) at  $3.4\ \text{\AA}$  but far from that of opal-A (PDF#38-0448) at  $4.08\ \text{\AA}$ , which indicates the presence of amorphous silica rather than opaline silica. In Fe0.9 and Fe1.0, the reflections increased remarkably in intensity but still remained a broad feature.

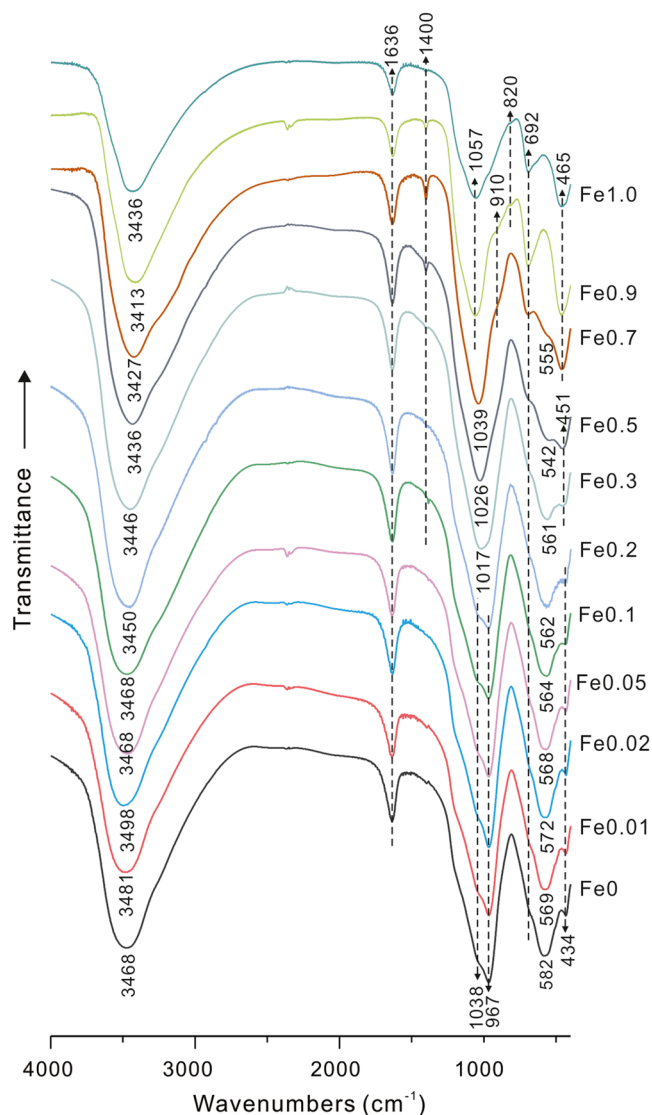


**Figure 2.** Fourier transform infrared spectra of products obtained at different initial Fe/(Fe + Al) molar ratios.

### 3.2. FTIR Results

FTIR spectroscopy has been one of the most widely used tools to study the structural Fe in aluminosilicate minerals. The FTIR spectra of the products are shown in Figure 2. The spectrum of Fe0 exhibited bands at 3,468, 1,636, 967, 692, 582, and 434  $\text{cm}^{-1}$ , which agreed well with those of natural allophane (Parfitt, 1990). The broad band centered at 3,468  $\text{cm}^{-1}$  was ascribed to the OH stretching vibration in allophane and the physisorbed water (Deng et al., 2019). The band at 1,636  $\text{cm}^{-1}$  originated from the H–O–H bending vibration in the physisorbed water (Murad & Bishop, 2000). The single band at 967  $\text{cm}^{-1}$  was ascribed to the Si–O stretching vibration and is characteristic of allophane (Du et al., 2020). A shoulder band appeared at 1,038  $\text{cm}^{-1}$ , which might be ascribed to the Si–O–Si stretching vibration in the oligomeric silica on the inner surface of allophane. The very weak shoulder band at 692  $\text{cm}^{-1}$  arose from imogolite local structure (ImoLS, curved gibbsite-like fragments with Al–OH on the inner side substituted by orthosilicate groups) and is characteristic of allophane-like materials (Du et al., 2017; Parfitt, 1990). The band at 582  $\text{cm}^{-1}$  was ascribed to the Al–O–Si deformation (Wang et al., 2018) and is characteristic of allophane. The band at 434  $\text{cm}^{-1}$  was ascribed to the O–Si–O bending vibration in allophane (Du et al., 2018).

At  $n \leq 0.2$ , the overall FTIR spectra of the products remained almost constant, indicating that the addition of a small amount of Fe brought limited changes to the structure and phases of the products and that allophane dominated the products, which was consistent with the XRD results. A band at 1,400  $\text{cm}^{-1}$  appeared in Fe0.1 and remained up to Fe1.0, of which the ascription was not straightforward. Significant changes were shown in the spectrum of Fe0.3. The band at 967  $\text{cm}^{-1}$  and the shoulder band at 1,038  $\text{cm}^{-1}$  were immersed into one single band at 1,017  $\text{cm}^{-1}$ . This new band arose from a combination of the Si–O stretching vibration in the allophane structure and the Si–O–Si stretching vibrations in both the oligomeric silica on the inner surface of allophane and the excess amorphous silica that was not attached to the allophane structure. It shifted to the higher-wavenumber side with increasing Fe content and reached a maximum at 1,057  $\text{cm}^{-1}$  in Fe0.9, after which it remained constant. This shift might be due to the continued formation of amorphous silica and thus the increased Si–O–Si/Si–O ratios. The band at 692  $\text{cm}^{-1}$  increased in intensity from Fe0.3 on. However, the assignment of this band gradually changed. At a medium or high Fe concentration, this band was mainly ascribed to the Fe–O asymmetric stretching vibration (Doelsch

et al., 2001) or to the H–O...Cl hydrogen bonds (Sun et al., 2013) in akaganeite. Murad and Bishop (2000) found that the intensity of this band was affected by the interaction between akaganeite and alkali halides. In addition, the band at 434  $\text{cm}^{-1}$  was shifted to 451  $\text{cm}^{-1}$  in Fe0.3. In the spectrum of Fe0.5, the band at 582  $\text{cm}^{-1}$  was shifted to 542  $\text{cm}^{-1}$  and transformed into a shoulder band, indicating that Fe-containing allophane or allophane-like materials no longer dominated Fe0.5, in good agreement with the XRD results. A shoulder band at 910  $\text{cm}^{-1}$  appeared in Fe0.7, decreased in intensity in Fe0.9 and disappeared in Fe1.0. This band might be ascribed to the bending vibration of Al<sub>2</sub>OH (Iriarte et al., 2005) of the Al–Si phases that were separated from the Fe phases. The band at 820  $\text{cm}^{-1}$  might be ascribed to the OH bending vibration of octahedral Fe (Murad & Bishop, 2000). Alternative ascriptions of this band are the libration modes of H–O...Cl hydrogen bonds or the Fe–O–Fe bridge in akaganeite (Gonzalezcalbet et al., 1981; Sugimoto et al., 1998). The O–Si–O bending band further increased to 465  $\text{cm}^{-1}$  in Fe 0.7, as observed by Doelsch et al. (2001) in the Si–Fe aggregates. In Fe1.0, which was dominated by akaganeite, the doublets near 3,344 and 3,442  $\text{cm}^{-1}$  that appeared in pure akaganeite (Barrero et al., 2006) were not observed, probably due to a combination

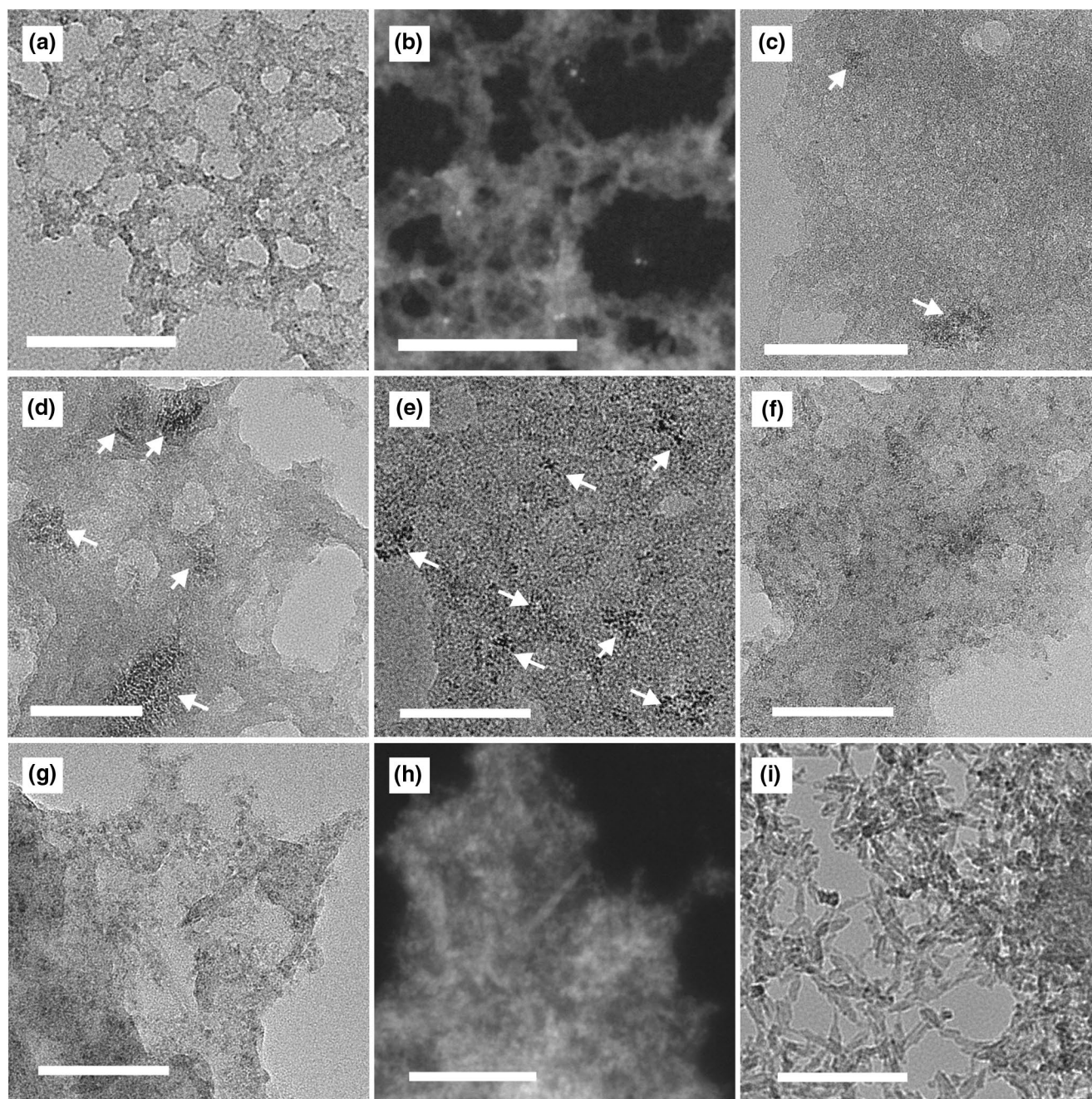


**Figure 3.** Transmission electron microscopy images of the selected products: Fe0 (a and b), Fe0.05 (c), Fe0.1 (d), Fe0.2 (e), Fe0.3 (f), Fe0.7 (g and h), and Fe1.0 (i). (a, c–g, and i) Bright field images; (b and h) dark field images. Scale bar: 100 nm.

of the presence of amorphous silica and the high hydration degree resulting from the low crystallinity of akaganeite.

### 3.3. TEM Observations

Changes in the microstructure, morphology and aggregation state of the selected products induced by introducing Fe were directly observed by TEM; the results are exhibited in Figure 3. The product Fe0 showed a cloud-like morphology (Figures 3a and 3b), which is characteristic of allophane (Ding et al., 2019). The hollow nanospherical structure of allophane was hardly observed due to a combination of small particle

sizes, low structural order and severe aggregation of the allophane particles (Du et al., 2020). Abundant porosity formed in and between the cloud-like aggregates, which endowed allophane with a high specific surface area.

Compared to Al and Si, Fe has a much larger atomic number and thus can be identified with ease in these products by its significantly higher contrast in the TEM images (blackier in the bright field images and whiter in the dark field images). At  $n = 0.05$ , Fe-containing clusters of several nanometers to several dozens of nanometers (indicated by arrows) appeared (Figure 3c). These clusters were distributed inhomogeneously in the clouds, in which Fe was believed to mainly substitute for Al, in combination with the XRD and FTIR results. The occurrence of these Fe-containing clusters was previously proposed based on the X-ray absorption fine structure data by Baker et al. (2014). The number of clusters increased up to  $n = 0.2$  (Figures 3a–3e). At  $n = 0.3$ , the Fe-containing clusters were almost absent; instead, the Fe phases began to separate from the Al-Si phases, forming Fe-rich domains of several nanometers, which were distributed relatively homogeneously in the clouds (Figure 3f). At  $n = 0.7$ , nanosized Fe-rich crystals, resulting from the crystallization of the Fe-rich domains, appeared in the products (Figures 3g and 3h), which were indexed to akaganeite by the XRD results (Figure 1). As Al was totally substituted by Fe, the product Fe1.0 was dominated by akaganeite with a spindle-like morphology, partly embraced by amorphous silica (Figure 3i). The akaganeite grains ranged in length and width from 15 to 30 nm and from 5 to 10 nm, respectively, smaller than most of those previously reported (e.g., Barrero et al., 2006; Bibi et al., 2011; Murad, 1979).

### 3.4. Mössbauer Spectra

To study the occurrence of Fe in the products, both room-temperature and low-temperature (12 K) Mössbauer spectra of the selected products were recorded, and the results (including the fitting parameters) are exhibited in Figures S1, 4, and Table S1. The room-temperature Mössbauer spectra of Fe0.05, Fe0.1, Fe0.3, and Fe1.0 were fit to two quadrupole doublets with IS values of 0.35 and 0.36 mm s<sup>-1</sup> (Figure S1, Table S1), indicating the presence of Fe<sup>3+</sup> cations at two different octahedral sites (Garten et al., 1970; Meagher et al., 1988). Little further information could be extracted, because the room-temperature Mössbauer spectra of iron (oxyhydr)oxides with very small particle sizes and/or very low crystallinity do not necessarily exhibit sextets (Fysh et al., 1983; Murad, 1987) and thus cannot be differentiated from those of structural Fe.

Fitting the low-temperature Mössbauer spectra of the products in this Al-Si-Fe system was very challenging because of (i) the heterogeneous distribution of structural Fe as nanoclusters in the products as revealed by the TEM results; (ii) the small particle sizes and low crystallinities of allophane, akaganeite and their precursors; and (iii) the complex Mössbauer spectra of both paramagnetically and magnetically ordered akaganeite due to the interactions between tunnel Cl<sup>-</sup> and the neighboring Fe<sup>3+</sup> ions (Childs et al., 1980; Murad, 1979). In early studies, the low-temperature Mössbauer spectrum of akaganeite was fit with three distinct Fe<sup>3+</sup> components based on the tetragonal I4/m symmetry (e.g., Murad, 1979; Rezel & Genin, 1990). However, more recent studies have suggested that the monoclinic I2/m symmetry is more reasonable than the I4/m symmetry (e.g., Post et al., 2003; Ståhl et al., 2003), and that there exist two distinct Fe<sup>3+</sup> sites that require four separate sextets to fit the low-temperature Mössbauer spectra (Barrero et al., 2006). Therefore, we tentatively fit the low-temperature Mössbauer spectra of Fe0.1, Fe0.2, and Fe0.3, in which both doublet and sextet components are shown, with two doublets and two sextets, assuming that the doublets arose from the structural Fe and the sextets arose from the concomitant iron (oxyhydr)oxides. The added area of the doublet components, compared to that of the sextet components, increased significantly with  $n$  (Figure 4, Table S1), suggesting that the proportion of structural Fe in allophane increased with  $n$ , contrary to our expectation. One possible reason for this paradox was that an increasing part of the doublet components was ascribed to the incipient akaganeite, which behaved superparamagnetically even at 12 K. We fit the low-temperature Mössbauer spectra of Fe1.0 with four sextets and a relaxation (R) component, of which the former arose from akaganeite while the latter might be due to the co-occurrence of amorphous silica and the Si-for-Fe substitution in akaganeite.

In spite of the abovementioned difficulties in interpreting the Mössbauer results, the presence of doublets in Fe0.1, Fe0.2, and Fe0.3 and their absence in Fe1.0 confirms, for the first time, that Fe was incorporated into the structure of allophane. Combined with the room-temperature Mössbauer data, these structural Fe were located at octahedral sites by substituting for structural Al. Moreover, the presence of sextets in Fe0.1

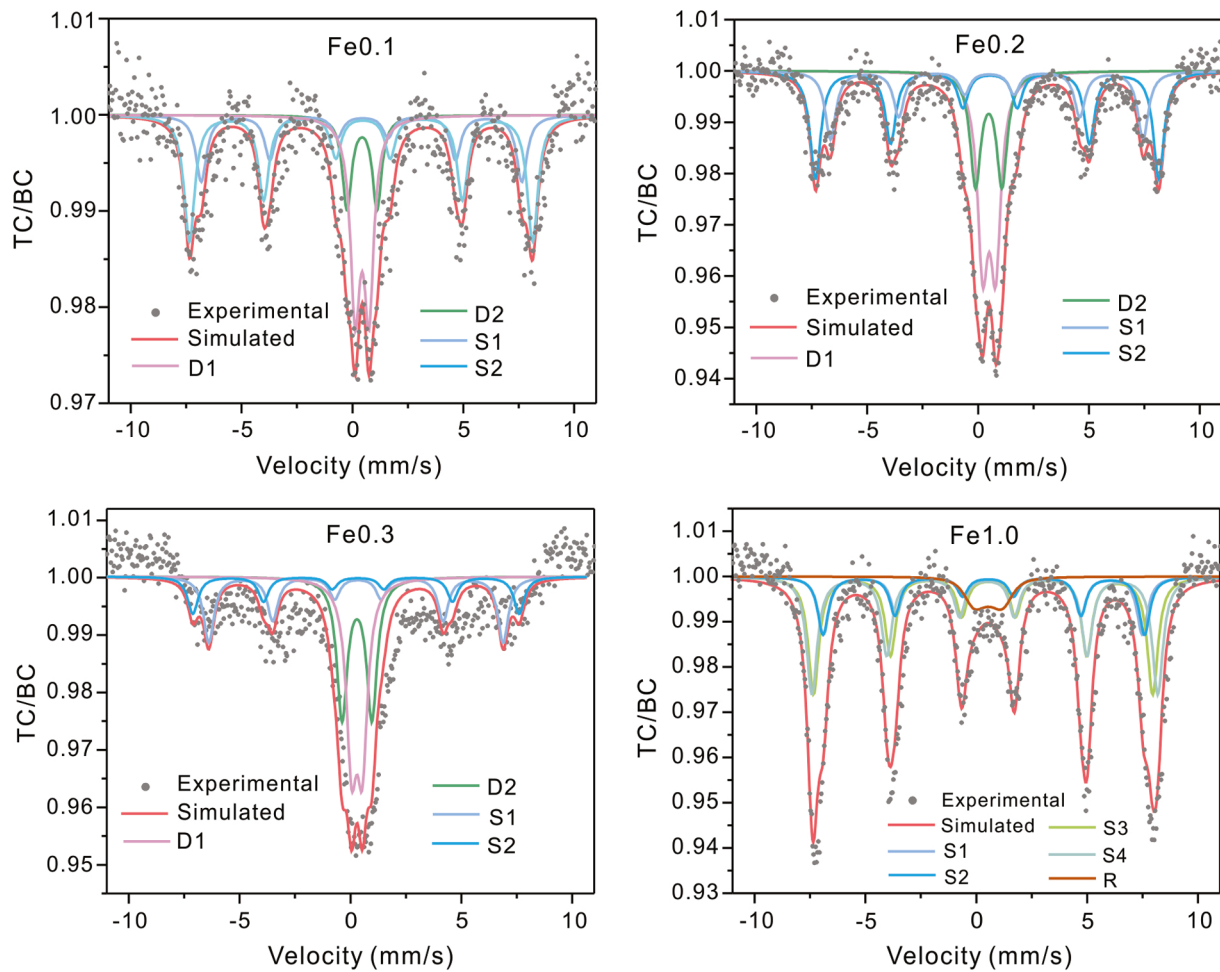


**Figure 4.** Low-temperature (12 K) Mössbauer spectra of the selected products. Note the poor fit to the outmost lines of the spectra is a result of relaxation effects. BC, baseline counts; TC, total counts.

and Fe0.2 suggested the occurrence of incipient akaganeite, which was hardly detected by XRD and FTIR techniques due to the small particle size and low crystallinity.

### 3.5. VNIR Spectra

The VNIR spectra of the products were recorded to follow the Fe-introduction-induced changes in the spectral features for possible comparative studies on Mars. The parameters were extracted from the spectra with the method presented by Clark and Roush (1984) and Viviano-Beck et al. (2014), which is detailed in Supporting Information S1, Figure S2 and Table S2. The results are shown in Figure 5. In the VNIR spectrum of Fe0, three bands were observed near 1.43, 1.92, and 2.20  $\mu\text{m}$ , which was consistent with allophane (Bishop et al., 2013). These bands were ascribed to the OH stretching overtones in both aluminosilicates and the adsorbed  $\text{H}_2\text{O}$ , a combination of OH bending and stretching vibrations in the adsorbed  $\text{H}_2\text{O}$  and a combination of stretching and bending vibrations of structural OH in aluminosilicates, respectively (Bishop et al., 2013). They were broad due to the distribution of Al–OH and Si–OH sites in the allophane structure (Bishop, 2018). In addition, two weak bands were observed at 0.97 and 1.15  $\mu\text{m}$ , of which the ascriptions were ambiguous. These two bands might be characteristic of allophane as their intensities evolved synchronously with the allophane contents in the products, in combination with the XRD and FTIR results.

In the VNIR spectrum of Fe0.01, a steep slope appeared below 0.59  $\mu\text{m}$ , with the presence of a small shoulder near 0.49  $\mu\text{m}$ . These features arose from  $\text{Fe}^{3+}$  electronic excitations (Bishop et al., 2015). As the Fe



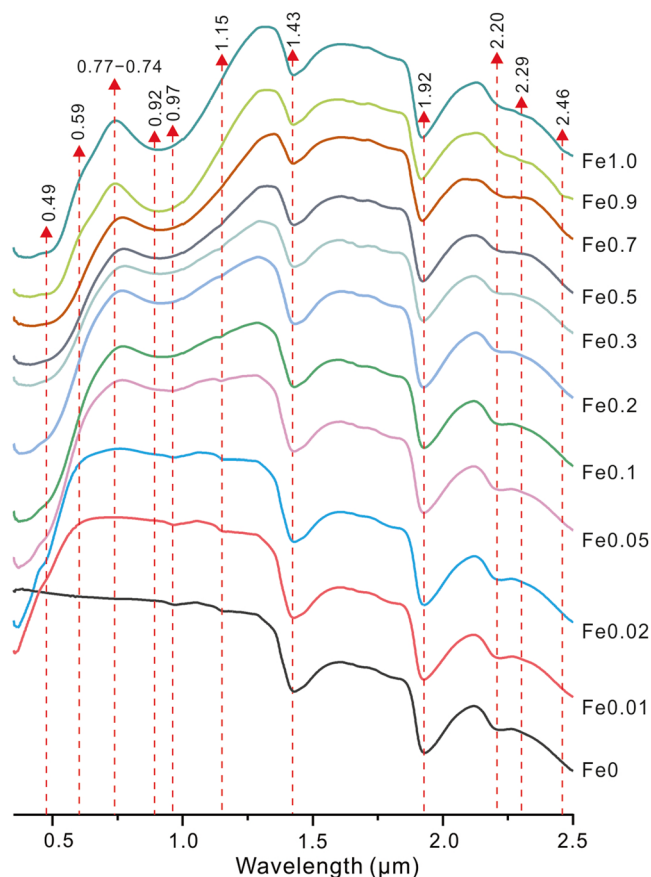


**Figure 5.** Visible and near-infrared spectra of the products obtained at different initial Fe/(Fe + Al) molar ratios.

concentrations increased, the features in the range of 0.4–1.2  $\mu\text{m}$  underwent significant changes, mainly including the presence and evolution of two broad absorption bands (reflectance minima) centered at 0.49 and 0.92  $\mu\text{m}$ . These two bands were separated by a reflectance maximum, of which the center ranged from 0.77 to 0.74  $\mu\text{m}$  with increasing Fe concentration. In Fe1.0, these features evolved into a broad band centered at approximately 0.92  $\mu\text{m}$ , a reflectance maximum near 0.74  $\mu\text{m}$  and a shoulder band near 0.59  $\mu\text{m}$ , in line with the features of akaganeite (Bishop et al., 2015). In contrast, the spectra in the range of 1.2–2.6  $\mu\text{m}$  exhibited fewer noticeable changes with increasing Fe concentration (Figure 5). At  $n \geq 0.3$ , a very weak band at 2.29  $\mu\text{m}$  appeared, which was attributed to the Fe–OH stretching plus bending vibrations (McKeown et al., 2009); at the same time, the Fe phases began to separate from the Al–Si phases (Figure 3f). At  $n \geq 0.9$ , a band at 2.46  $\mu\text{m}$  was observed, which was attributed to the OH combination stretching plus out-of-plane bending vibration for OH groups that were associated with the tunnel  $\text{Cl}^-$  in akaganeite (Bishop et al., 2015), suggesting the dominance of akaganeite. This band, which frequently appears with several shoulder bands in the 2.25–2.42  $\mu\text{m}$  range (Peretyazhko et al., 2019), such as the band at 2.37  $\mu\text{m}$  in this case, has been widely used to detect akaganeite on Mars (e.g., Bishop, 2018; Bishop et al., 2015).

## 4. Discussions

### 4.1. Effects of Environmental Fe Concentrations on Allophane Formation

Environmental Fe can be incorporated into the allophane structure by substituting for structural Al and/or coated on the allophane surface in the form of iron (oxyhydr)oxides, such as akaganeite in Cl-rich environments, as reported in this study, in the formation of allophane. Specifically, at low Fe concentrations ( $n \leq 0.2$ ), Fe-rich allophane was formed, with Fe mainly substituting for octahedrally coordinated Al in the gibbsite-like sheets, resulting in increased decreases of crystallinity. This substitution is confirmed by the presence of doublets in the low-temperature (12 K) Mössbauer spectra (Figure 4). At the nanoscale, the structural Fe appeared as nanoclusters due to the easy formation of Fe–O–Fe bonds, which were distributed heterogeneously in the products (Figures 3a–3e). This scenario is in contrast to the case of other aluminosilicates such as kaolinite, where Fe and Al coexist in a solid solution without any discontinuity (Iriarte et al., 2005). This discrepancy might be partly explained by the much larger precipitation rate and much lower per se structural order of allophane than those of kaolinite.

As the Fe concentration increases, the formation of allophane is increasingly suppressed. At  $n = 0.3$ , Fe-containing allophane or allophane-like materials might still dominate the product, as shown by the XRD results. Combined with the FTIR results, Fe-containing allophane dominated Fe0.2 and were probably the main phase in Fe0.3. Based on this, the highest Fe-for-Al substitution content in allophane was roughly estimated to be  $\sim 20$  mol.%. The low-temperature Mössbauer spectrum of Fe0.1 seems to suggest the presence of a significant amount of akaganeite in Fe0.1. However, as explained above, the low-temperature Mössbauer spectra are difficult to fit and thus provide limited quantitative information. The utmost substitution content is much higher than the values previously reported. Ossaka et al. (1971) suggested that the highest content of structural Fe in allophane was 5 wt.% ( $\sim 12$  mol.% Fe-for-Al substitution, calculated from a assumed formula of  $\text{SiO}_2 \cdot \text{Al}_{2-x}\text{Fe}_x\text{O}_3 \cdot 5\text{H}_2\text{O}$ ), while Baker et al. (2014) found that at most 1 mol.% Al can be substituted by Fe. The Fe phases began to separate from the Al–Si phases in Fe0.3. At  $n = 0.5$ , only a small number, if any, of Fe-containing allophane or allophane-like materials were formed, together with an increased amount of nanosized incipient akaganeite. At  $n = 0.7$ , allophane was no longer formed, probably

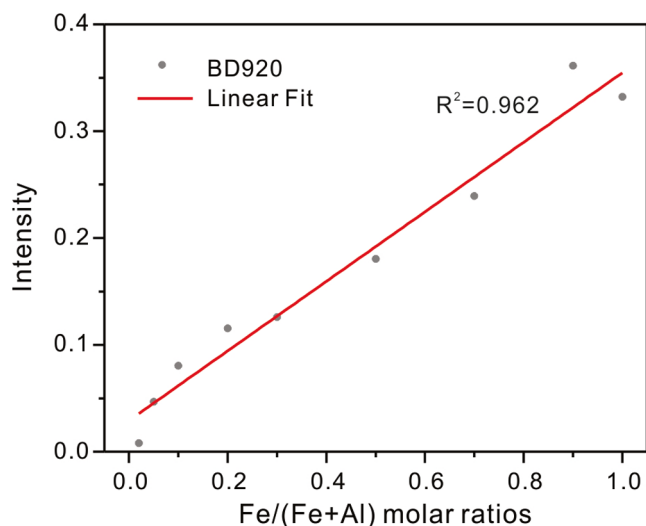


**Figure 6.** Band depth ( $0.92 \mu\text{m}$ ) as a function of Fe/(Fe + Al) molar ratios.

due to disadvantageous conditions such as a dramatically decreased pH (at  $0 \leq n \leq 0.3$ ,  $3.08 \leq \text{pH} \leq 3.38$ ; at  $n = 0.5$ ,  $\text{pH} = 2.75$ ; and at  $n = 0.7$ ,  $\text{pH} = 2.07$ ; pH being measured after hydrothermal treatments). The Al atoms might exist in amorphous hydroxyl-rich Al phases or Al-Si phases, as suggested by the presence of the FTIR band at  $910 \text{ cm}^{-1}$  in the FTIR spectrum. The excess Si probably forms amorphous silica. As the Fe concentration further increases, the crystallization and growth of spindle-like akaganeite occur.

#### 4.2. Factors Controlling the Formation and Crystallization of Akaganeite

Akaganeite was obtained at a high concentration of  $\text{SiO}_2$  sol (together with a certain amount of  $\text{Al}_2\text{O}_3$  and aluminosilicate sols in some cases), suggesting the easy formation of akaganeite in Cl-rich conditions. However, in conditions rich in other anions such as nitrate (Colombo & Violante, 1996) and  $\text{ClO}_4^-$  (Mcbride et al., 1984), other iron (oxyhydr)oxides (e.g., ferrihydrite, hematite) were formed in the Fe-Si hydrolysis systems. These results suggested that the presence and species of anions rather than of other inorganic sols controlled the species of as-formed iron (oxyhydr)oxides.

On the other hand, the akaganeite crystals obtained in this study are much smaller than most of those obtained under Si-free conditions. One possible reason is that the presence of amorphous silica (and Al-Si phases) limited the crystallization of akaganeite. Similar suppressing effects of  $\text{SiO}_2$  sol on the formation of other iron (oxyhydr)oxides, such as goethite (Kandori et al., 1992), have been reported. Moreover, natural ferrihydrite normally, if not invariably, contains silica (Mcbride et al., 1984), indicating that the presence of silica might prevent it from transforming into more crystalline iron (oxyhydr)oxides (Cornell et al., 1987). However, the presence of  $\text{SiO}_2$  sol, in some other cases, may have limited suppression and even promoted effects on the formation of ferrihydrite (Schwertmann & Thalmann, 1976) and akaganeite (Ishikawa et al., 2005).

#### 4.3. Use of VNIR Spectroscopy in the Detection of Fe-Containing Phases

VNIR spectroscopy has been the most commonly used technique to detect the mineralogy of Mars (Bishop, 2018). The features near  $1.40$ ,  $1.90$ , and  $2.20 \mu\text{m}$ , produced by the overtones and combinations of OH and  $\text{H}_2\text{O}$ , are commonly used to identify mineral species. The band near  $2.20 \mu\text{m}$  exhibits significant changes with different chemical compositions and structures of aluminosilicates and was the main basis for mineralogical identification (Bishop, 2018; Cuadros et al., 2016). The band near  $1.40 \mu\text{m}$  exhibits a slight variation as a function of the octahedral compositions of the aluminosilicates and was of secondary significance in discriminating between them (Cuadros et al., 2016). However, for Fe-rich allophane ( $n \leq 0.3$ ), no appreciable shifts for the bands at  $1.43$ ,  $1.92$ , and  $2.20 \mu\text{m}$  as a function of Fe content were observed; the depths of the bands near  $1.43$  and  $2.20 \mu\text{m}$  slightly decrease overall (Figures 5 and S3, Table S2). These results indicate that the identification of amorphous and short-range ordered hydrated minerals in the Al-Si-Fe system based on the VNIR data ( $1.2\text{--}2.6 \mu\text{m}$ ) might be questionable. However, the spectra in the range of  $0.4\text{--}1.2 \mu\text{m}$  are very sensitive to the Fe contents of the products. Even if 1% of the Al atoms are substituted by Fe atoms, the electronic excitation bands at  $0.4\text{--}0.5 \mu\text{m}$  appear. With the increase in Fe contents in the products, significant changes occurred in this spectral range. At  $n = 1.0$ , the bands in this range are characteristic of akaganeite (Figure 5). Moreover, the depth of the band near  $0.92 \mu\text{m}$  (BD920) increased proportionately with the total Fe contents of the products (Figure 6). These results suggested that Fe electronic excitation bands can be used to detect a small amount of Fe in aluminosilicate minerals, to qualitatively identify iron (oxyhydr)oxides and to quantify the total Fe in soils and sediments and thus should always be considered in the analysis of the mineralogy and chemistry of Mars. Notably, the VNIR data of the products provide references for studying the short-range ordered phases in the Al-Si-Fe systems.

## 5. Implications

### 5.1. On the Matter Cycle in the Al-Si-Fe Systems

The weathering of silicates supplies a range of ions (mainly  $\text{Al}^{3+}$ ,  $\text{Si}^{4+}$ , and  $\text{Fe}^{3+}$ , also  $\text{Ca}^{2+}$ ,  $\text{Mg}^{2+}$ ,  $\text{Fe}^{2+}$ ,  $\text{Na}^+$ ,  $\text{K}^+$ , and  $\text{Mn}^{4+}$ ) to the soil solutions (Tamrat et al., 2019). Thus, Al-Si-Fe systems are one of the most commonly encountered systems in weathering environments, both on Earth (Naren et al., 2013) and on Mars (McLennan, 2003). In these systems, short-range ordered minerals such as allophane often prevail. In some conditions where acidic pH occurs,  $\text{Fe}^{3+}$  is mobile and available for incorporation into the allophane structure. The findings presented here, that is, (1)  $\text{Al}_2\text{O}_3$  sol, compared to  $\text{Fe}_2\text{O}_3$  sol, is prone to react with  $\text{SiO}_2$  sol to form allophane at a low or moderate  $n$  and (2) the presence and species of the anions control the species of the associated iron (oxyhydr)oxides, reveal the formation and transition of minerals in the Al-Si-Fe system. In addition, the occurrence of structural Fe in allophane might lower its stability (Wilson et al., 2006), affecting its preservation, dissolution and transformation into other minerals and thus affecting the geochemical cycle of Al, Si, and Fe in weathering environments.

On the other hand, allophane plays an important role in controlling the sequestration, transport and fate of heavy metals, anions, radioactive elements and organic matter in the occurrence environments due to its high specific surface area, variable surface charge and potentially large number of sorption sites (Wada, 1989). The occurrence of structural Fe in allophane will transform a certain amount of Al–OH and Si–OH on the particle surface into Fe–OH, resulting in changes in the surface charge. Moreover, structural Fe probably endows allophane with a unique catalytic reactivity (Garrido-Ramírez et al., 2013) or provides coordination centers for specific atoms (e.g., N atoms) of certain organic molecules (Tamrat et al., 2019), affecting the roles of allophane in the interfacial adsorption and degradation of guest molecules (Ding et al., 2019). For example, the occurrence of a large amount of Fe-rich allophane in soils was considered to increase the amount of active groups on the soil particle surface, promoting the formation of highly stable mineral-organic complexes in soils (Filimonova et al., 2016). In addition, even iron (oxyhydr)oxide coatings on the particles or microaggregates of allophane result in changes in the properties of these particles (Silva-Yumi et al., 2018). Therefore, the environmental Fe concentration is a key factor that controls the formation and evolution of allophane and thus has an important influence on the migration and cycle of matter in Al-Si-Fe systems.

### 5.2. On the Paleoenvironment of Locations Where Allophane and Akaganeite Co-Occur

In many geological environments and geologic bodies, aluminosilicate minerals, and iron (oxyhydr)oxides are known to associate closely rather than occur as separate entities, both on Earth and on Mars (Kaplan et al., 2016; Lefticariu et al., 2017), and these two kinds of minerals, at least in some cases, likely form around the same time. However, the formation and evolution of clay-rich and Fe-rich formations are generally considered separate geological events on both Earth and Mars, in which no interaction occurs during and after their initial formation (Bowman & Lefticariu, 2018). In this study, allophane and akaganeite are formed as a function of Fe concentrations in similar hydrothermal environments, providing a chance to study their co-occurrence and the involved geological significance.

On Earth, akaganeite often appears as the corrosion product of metallic Fe or Fe(II) in acidic Cl-rich oxidation conditions (Bibi et al., 2011) and has been found in Cl-rich environments including soils drained of acidic water, hot brines, marine environments, sediment of sulfur-rich oxides, carbonate concretion, Fe-Ni meteorites and even Fe-rich archeological sites (Buchwald & Clarke, 1989; Font et al., 2017; Réguer et al., 2007). These conditions are distinctly different from the conditions under which allophane typically occurs. In fact, the co-occurrence of allophane and akaganeite on Earth has rarely been reported. However, allophane and akaganeite might co-occur in several locations on Mars. Both of them have been detected in Rocknest aeolian deposit (Beaty et al., 2016; Bish et al., 2013; Blake et al., 2013), although they might be brought together after their formation. Akaganeite has been identified in the mudstone samples drilled from Yellowknife Bay and Vera Rubin ridge, of which the amorphous components might also contain allophane (Rampe et al., 2020; Vaniman et al., 2014). The fact that Mars' crust has a higher Fe abundance than that of Earth's crust (McLennan, 2003) might partly explain the discrepancy of the co-occurrence of allophane and akaganeite on Earth and on Mars because higher  $n$  are expected to be more common on Mars surface.

In this study,  $n$  was found to be a major factor that controls the phases in the Al-Si-Fe systems. A moderate  $n$  ( $0.3 \leq n \leq 0.5$ ) permits the co-occurrence of allophane and akaganeite. At a lower  $n$  (e.g.,  $n \leq 0.2$ ), Fe is likely to be mainly incorporated into the allophane structure. At a higher  $n$  (e.g.,  $n \geq 0.7$ ), allophane cannot be formed due to a dramatic decrease of pH. Although a high temperature and high concentrations were used in this study, they were believed to increase the reaction rate and the yields rather than to control the as-obtained products. As  $n$  increases from 0 to 1, (incipient) akaganeite was the only iron (oxyhydr)oxides obtained in this Cl-rich system. In combination with the above knowledge and the respective typical occurrence environments of allophane and akaganeite on Earth, their co-occurrence on Mars would indicate the presence of a Cl-rich Al-Si-Fe system with a moderate  $n$ , where a moderate to weakly acidic oxidative environment prevailed. In addition, the presence of these two poorly crystallized materials indicates that little aqueous or thermal alteration of the surface materials has taken place after their formation, probably due to a persistently dry climate, which delays the transformation from these phases into well-crystallized clay minerals (e.g., halloysite) and iron (oxyhydr)oxides such as hematite (Fu et al., 2020), respectively.

## 6. Conclusions

Environmental Fe concentrations control the formation and evolution of allophane in Al-Si-Fe systems. At low- and medium-Fe concentrations, allophane was formed, and Fe was incorporated into the allophane structure and/or formed iron (oxyhydr)oxide coatings on the allophane surface. The proportion of structural Fe decreased with increasing Fe concentration. The presence of structural Fe lowered the crystallinity of allophane. Approximately 20 mol.% Al, at most, was roughly estimated to be substituted by Fe, much higher than previously reported. At high Fe concentrations, allophane was no longer formed, and iron (oxyhydr)oxides (akaganeite in Cl-rich conditions) were crystallized from the Fe phases in association with amorphous phases such as amorphous silica. The VNIR spectra of the products suggest the weakness of the VNIR features in the range of 1.2–2.6  $\mu\text{m}$  in the detection of short-range ordered minerals in the Al-Si-Fe system. Instead, Fe electronic excitation bands in the range of 0.4–1.2  $\mu\text{m}$  can be used to detect a small amount of Fe in aluminosilicates, to identify the species of iron (oxyhydr)oxides and to quantify the total Fe in soils or sediments. These findings not only offer insight into the formation, evolution, and geological role of allophane in supergene weathering environments as a function of the environmental Fe concentrations on Earth but also help identify the short-range ordered minerals and further constrain the local paleoenvironment on Mars.

## Data Availability Statement

All the experimental raw data are available from the figshare with the identifier (10.6084/m9.figshare.13139660.v1). This is a contribution (No. IS-2932) from GIGCAS.

## Acknowledgments

Financial supports from the National Special Support for High-Level Personnel, National Natural Science Foundation of China (41672042, 41972045, and 42002033) and Natural Science Foundation of Guangdong Province, China (2019A1515011957) are gratefully acknowledged.

## References

- Al-Samir, M., Nabhan, S., Fritz, J., Winkler, A., Bishop, J. L., Gross, C., et al. (2017). The paleolacustrine evolution of Juventae Chasma and Maja Valles and its implications for the formation of interior layered deposits on Mars. *Icarus*, 292, 125–143. <https://doi.org/10.1016/j.icarus.2016.12.023>
- Baker, L. L., Nickerson, R. D., & Strawn, D. G. (2014). XAFS study of Fe-substituted allophane and imogolite. *Clays and Clay Minerals*, 62(1), 20–34. <https://doi.org/10.1346/ccmn.2014.0620103>
- Barrero, C. A., García, K. E., Morales, A. L., Kodjikian, S., & Greneche, J. M. (2006). New analysis of the Mössbauer spectra of akaganeite. *Journal of Physics: Condensed Matter*, 18(29), 6827–6840. <https://doi.org/10.1088/0953-8984/18/29/020>
- Beatty, D., Abud-Madrid, A., Boucher, D., Bussey, B., Davis, R., Gertsch, L., et al. (2016). Description of water resources on Mars that have the potential to become reserves as part of a human exploration zone: The m-wip study, part 1. In *Paper presented at the Space Resources Roundtable*, Golden, CO.
- Bibi, I., Singh, B., & Silvester, E. (2011). Akaganeite ( $\beta$ -FeOOH) precipitation in inland acid sulfate soils of south-western New South Wales (NSW), Australia. *Geochimica et Cosmochimica Acta*, 75(21), 6429–6438. <https://doi.org/10.1016/j.gca.2011.08.019>
- Bish, D. L., Blake, D. F., Vaniman, D. T., Chipera, S. J., Morris, R. V., Ming, D. W., et al. (2013). X-ray diffraction results from mars science laboratory: Mineralogy of rocknest at Gale Crater. *Science*, 341(6153), 1238932. <https://doi.org/10.1126/science.1238932>
- Bishop, J. L. (2018). Remote detection of phyllosilicates on Mars and implications for climate and habitability. In N. A. Cabrol, & E. A. Grin (Eds.), *From habitability to life on Mars* (pp. 37–75). Amsterdam, the Netherlands: Elsevier.
- Bishop, J. L., Fairen, A. G., Michalski, J. R., Gago-Duport, L., Baker, L. L., Velbel, M. A., et al. (2018). Surface clay formation during short-term warmer and wetter conditions on a largely cold ancient Mars. *Nature Astronomy*, 2(3), 206–213. <https://doi.org/10.1038/s41550-017-0377-9>
- Bishop, J. L., Murad, E., & Dyar, M. D. (2015). Akaganeite and schwertmannite: Spectral properties and geochemical implications of their possible presence on Mars. *American Mineralogist*, 100(4), 738–746. <https://doi.org/10.2138/am-2015-5016>

- Bishop, J. L., & Rampe, E. B. (2016). Evidence for a changing Martian climate from the mineralogy at Mawrth Vallis. *Earth and Planetary Science Letters*, 448, 42–48. <https://doi.org/10.1016/j.epsl.2016.04.031>
- Bishop, J. L., Rampe, E. B., Bish, D. L., Abidin, Z., Baker, L. L., Matsue, N., et al. (2013). Spectral and hydration properties of allophane and imogolite. *Clays and Clay Minerals*, 61(1), 57–74. <https://doi.org/10.1346/CCMN.2013.0610105>
- Blake, D. F., Morris, R. V., Kocurek, G., Morrison, S. M., Downs, R. T., Bish, D., et al. (2013). Curiosity at Gale Crater, Mars: Characterization and analysis of the Rocknest sand shadow. *Science*, 341(6153), 1239505. <https://doi.org/10.1126/science.1239505>
- Bowman, R., & Leticariu, L. (2018). Characterization of mixed-mineral systems involving clay and iron oxyhydroxide minerals under acidic conditions. In *Paper presented at the 49th Lunar and Planetary Science Conference*, The Woodlands, TX.
- Buchwald, V. F., & Clarke, R. S. (1989). Corrosion of Fe-Ni alloys by Cl-containing akaganeite (beta-FeOOH) - the Antarctic meteorite case. *American Mineralogist*, 74(5–6), 656–667.
- Chamley, H. (1989). *Clay sedimentology*. Berlin: Springer.
- Childs, C., Goodman, B., Paterson, E., & Woodhams, F. (1980). The nature of iron in akaganeite ( $\beta$ -FeOOH). *Australian Journal of Chemistry*, 33(1), 15–26. <https://doi.org/10.1071/CH9800015>
- Clark, R. N., & Roush, T. L. (1984). Reflectance spectroscopy: Quantitative analysis techniques for remote sensing applications. *Journal of Geophysical Research*, 89(B7), 6329–6340. <https://doi.org/10.1029/JB089iB07p06329>
- Colman, S. M. (1982). Clay mineralogy of weathering rinds and possible implications concerning the sources of clay minerals in soils. *Geology*, 10(7), 370–375. [https://doi.org/10.1130/0091-7613\(1982\)10<370:CMOWRA>2.0.CO;2](https://doi.org/10.1130/0091-7613(1982)10<370:CMOWRA>2.0.CO;2)
- Colombo, C., & Violante, A. (1996). Effect of time and temperature on the chemical composition and crystallization of mixed iron and aluminum species. *Clays and Clay Minerals*, 44(1), 113–120. <https://doi.org/10.1346/CCMN.1996.0440110>
- Cornell, R. M., Giovanoli, R., & Schindler, P. W. (1987). Effect of silicate species on the transformation of ferrihydrite into goethite and hematite in alkaline media. *Clays and Clay Minerals*, 35(1), 21–28. <https://doi.org/10.1346/ccmn.1987.0350103>
- Cornell, R. M., & Schwertmann, U. (2003). *The iron oxides: Structure, properties, reactions, occurrences and uses*. John Wiley & Sons.
- Cuadros, J., Michalski, J. R., Dekov, V., & Bishop, J. L. (2016). Octahedral chemistry of 2:1 clay minerals and hydroxyl band position in the near-infrared: Application to Mars. *American Mineralogist*, 101(3), 554–563. <https://doi.org/10.2138/am-2016-5366>
- Deng, L., Du, P., Yu, W., Yuan, P., Annabi-Bergaya, F., et al. (2019). Novel hierarchically porous allophane/diatomite nanocomposite for benzene adsorption. *Applied Clay Science*, 168, 155–163. <https://doi.org/10.1016/j.clay.2018.11.007>
- Ding, Y., Lu, Y., Liao, P., Peng, S., Liang, Y., Lin, Z., et al. (2019). Molecular fractionation and sub-nano scale distribution of dissolved organic matter on allophane. *Environmental Sciences: Nano*, 6, 2037–2048. <https://doi.org/10.1039/C9EN00335E>
- Doelsch, E., Rose, J., Masion, A., Bottero, J. Y., Nahon, D., & Bertsch, P. M. (2000). Speciation and crystal chemistry of iron (III) chloride hydrolyzed in the presence of SiO<sub>4</sub> ligands. 1. An Fe K-edge EXAFS study. *Langmuir*, 16(10), 4726–4731. <https://doi.org/10.1021/la991378h>
- Doelsch, E., Stone, W. E., Petit, S., Masion, A., Rose, J., Bottero, J.-Y., et al. (2001). Speciation and crystal chemistry of Fe (III) chloride hydrolyzed in the presence of SiO<sub>4</sub> ligands. 2. Characterization of Si–Fe aggregates by FTIR and <sup>29</sup>Si solid-state NMR. *Langmuir*, 17(5), 1399–1405. <https://doi.org/10.1021/la0013188>
- Du, P., Thill, A., Yuan, P., Wang, S., Liu, D., Gobeaux, F., et al. (2020). Tailoring structure and surface chemistry of hollow allophane nanospheres for optimization of aggregation by facile methyl modification. *Applied Surface Science*, 510, 145453. <https://doi.org/10.1016/j.apsusc.2020.145453>
- Du, P., Yuan, P., Liu, D., Wang, S., Song, H., & Guo, H. (2018). Calcination-induced changes in structure, morphology, and porosity of allophane. *Applied Clay Science*, 158, 211–218. <https://doi.org/10.1016/j.clay.2018.03.035>
- Du, P., Yuan, P., Thill, A., Annabi-Bergaya, F., Liu, D., & Wang, S. (2017). Insights into the formation mechanism of imogolite from a full-range observation of its sol-gel growth. *Applied Clay Science*, 150, 115–124. <https://doi.org/10.1016/j.clay.2017.09.021>
- Ehlmann, B. L., & Edwards, C. S. (2014). Mineralogy of the martian surface. *Annual Review of Earth and Planetary Sciences*, 42, 291–315. <https://doi.org/10.1146/annurev-earth-060313-055024>
- Ehlmann, B. L., Mustard, J. F., Murchie, S. L., Bibring, J. P., Meunier, A., Fraeman, A. A., et al. (2011). Subsurface water and clay mineral formation during the early history of Mars. *Nature*, 479(7371), 53–60. <https://doi.org/10.1038/nature10582>
- Farmer, V. C., Krishnamurti, G. S. R., & Huang, P. M. (1991). Synthetic allophane and layer-silicate formation in SiO<sub>2</sub>-Al<sub>2</sub>O<sub>3</sub>-FeO-Fe<sub>2</sub>O<sub>3</sub>-MgO-H<sub>2</sub>O systems at 23°C and 89°C in a calcareous environment. *Clays and Clay Minerals*, 39(6), 561–570. <https://doi.org/10.1346/Ccmn.1991.0390601>
- Filimonova, S., Kaufhold, S., Wagner, F. E., Häusler, W., & Kögel-Knabner, I. (2016). The role of allophane nano-structure and Fe oxide speciation for hosting soil organic matter in an allophanic Andosol. *Geochimica et Cosmochimica Acta*, 180, 284–302. <https://doi.org/10.1016/j.gca.2016.02.033>
- Font, E., Carlu, J., Remazeilles, C., Mather, T. A., Nedelec, A., Mirao, J., et al. (2017). End-Cretaceous akaganeite as a mineral marker of Deccan volcanism in the sedimentary record. *Scientific Reports*, 7, 11453. <https://doi.org/10.1038/s41598-017-11954-y>
- Fraeman, A. A., Arvidson, R. E., Catalano, J. G., Grotzinger, J. P., Morris, R. V., Murchie, S. L., et al. (2013). A hematite-bearing layer in Gale Crater, Mars: Mapping and implications for past aqueous conditions. *Geology*, 41(10), 1103–1106. <https://doi.org/10.1130/G34613.1>
- Fu, X., Jia, L., Wang, A., Cao, H., Ling, Z., Liu, C., et al. (2020). Thermal stability of akaganeite and its desiccation process under conditions relevant to Mars. *Icarus*, 336, 113435. <https://doi.org/10.1016/j.icarus.2019.113435>
- Fysh, S. A., Cashion, J. D., & Clark, P. E. (1983). Mössbauer effect studies of iron in kaolin. I. Structural iron. *Clays and Clay Minerals*, 31(4), 285–292. <https://doi.org/10.1346/ccmn.1983.0310406>
- Garrido-Ramírez, E., Mora, M., Marco, J., & Ureta-Zañartu, M. (2013). Characterization of nanostructured allophane clays and their use as support of iron species in a heterogeneous electro-Fenton system. *Applied Clay Science*, 86, 153–161. <https://doi.org/10.1016/j.clay.2013.10.001>
- Garten, R. L., Delgass, W. N., & Boudart, M. (1970). A Mössbauer spectroscopic study of the reversible oxidation of ferrous ions in Y zeolite. *Journal of Catalysis*, 18(1), 90–107. [https://doi.org/10.1016/0021-9517\(70\)90316-7](https://doi.org/10.1016/0021-9517(70)90316-7)
- Gendrin, A., Mangold, N., Bibring, J.-P., Langevin, Y., Gondet, B., Poulet, F., et al. (2005). Sulfates in martian layered terrains: The OMEGA/Mars express view. *Science*, 307(5715), 1587–1591. <https://doi.org/10.1126/science.1109087>
- Gonzalezcalbet, J. M., Alariofranco, M. A., & Gayosoandrade, M. (1981). The porous structure of synthetic akaganeite. *Journal of Inorganic and Nuclear Chemistry*, 43(2), 257–264. [https://doi.org/10.1016/0022-1902\(81\)90006-3](https://doi.org/10.1016/0022-1902(81)90006-3)
- Harsh, J. (2012). Poorly crystalline aluminosilicate clay minerals. In P. M. Huang, Y. Li, & M. E. Sumner (Eds.), *Handbook of soil sciences* (pp. 23.21–23.13). Boca Raton, FL: CRC Press.
- Holzwarth, U., & Gibson, N. (2011). The Scherrer equation versus the 'Debye-Scherrer equation. *Nature Nanotechnology*, 6(9), 534. <https://doi.org/10.1038/nnano.2011.145>

- Horikawa, Y., & Soezima, H. (1977). State analysis of iron in allophanic clays. II. Iron L-emission band spectra from allophanic clays and hisingerite by the use of an X-ray microanalyzer. *Clay Science*, 5(2), 97–102. <https://doi.org/10.11362/jcssjclayscience1960.5.97>
- Iriarte, B., Petit, S., Huertas, F. J., Fiore, S., Grauby, O., Decarreau, A., et al. (2005). Synthesis of kaolinite with a high level of Fe(3+) for Al substitution. *Clays and Clay Minerals*, 53(1), 1–10. <https://doi.org/10.1346/CCMN.2005.0530101>
- Ishikawa, T., Miyamoto, S., Kandori, K., & Nakayama, T. (2005). Influence of anions on the formation of beta-FeOOH rusts. *Corrosion Science*, 47(10), 2510–2520. <https://doi.org/10.1016/j.corsci.2004.10.016>
- Kandori, K., Uchida, S., Kataoka, S., & Ishikawa, T. (1992). Effects of silicate and phosphate ions on the formation of ferric oxide hydroxide particles. *Journal of Materials Science*, 27(3), 719–728. <https://doi.org/10.1007/pl00020655>
- Kaplan, H. H., Milliken, R. E., Fernández-Remolar, D., Amils, R., Robertson, K., et al. (2016). Orbital evidence for clay and acidic sulfate assemblages on Mars based on mineralogical analogs from Rio Tinto, Spain. *Icarus*, 275, 45–64. <https://doi.org/10.1016/j.icarus.2016.03.019>
- Kaufhold, S., Kaufhold, A., Jahn, R., Brito, S., Dohrmann, R., Hoffmann, R., et al. (2009). A new massive deposit of allophane raw material in Ecuador. *Clays and Clay Minerals*, 57(1), 72–81. <https://doi.org/10.1346/Ccmn.2009.0570107>
- Kitagawa, Y. (1973). Substitution of aluminum by iron in allophane. *Clay Science*, 4(4), 151–154.
- Lefticariu, L., Sutton, S. R., Bender, K. S., Lefticariu, M., Pentrak, M., & Stucki, J. W. (2017). Impacts of detrital nano- and micro-scale particles (dNP) on contaminant dynamics in a coal mine AMD treatment system. *The Science of the Total Environment*, 575, 941–955. <https://doi.org/10.1016/j.scitotenv.2016.09.154>
- Levard, C., & Basile-Doelsch, I. (2016). Geology and mineralogy of imogolite-type materials. In P. Yuan, A. Thill, & F. Bergaya (Eds.), *Nanosized tubular clay minerals* (pp. 49–65). Amsterdam, the Netherlands: Elsevier.
- Mcbride, M. B., Farmer, V. C., Russell, J. D., Tait, J. M., & Goodman, B. A. (1984). Iron substitution in aluminosilicate sols synthesized at low pH. *Clay Minerals*, 19(1), 1–8. <https://doi.org/10.1180/claymin.1984.019.1.01>
- McKeown, N. K., Bishop, J. L., Dobrea, E. Z. N., Ehlmann, B. L., Parente, M., Mustard, J. F., et al. (2009). Characterization of phyllosilicates observed in the central Mawrth Vallis region, Mars, their potential formational processes, and implications for past climate. *Journal of Geophysical Research*, 114, e2008je003301. <https://doi.org/10.1029/2008je003301>
- McLennan, S. M. (2003). Sedimentary silica on Mars. *Geology*, 31(4), 315–318. [https://doi.org/10.1130/0091-7613\(2003\)031<0315:Som>2.0.Co;2](https://doi.org/10.1130/0091-7613(2003)031<0315:Som>2.0.Co;2)
- Meagher, A., Nair, V., & Szostak, R. (1988). A Mössbauer study of ZSM-5-type ferrisilicates. *Zeolites*, 8(1), 3–11. [https://doi.org/10.1016/S0144-2449\(88\)80022-8](https://doi.org/10.1016/S0144-2449(88)80022-8)
- Ming, D. W., Mittlefehldt, D. W., Morris, R. V., Golden, D. C., Gellert, R., Yen, A., et al. (2006). Geochemical and mineralogical indicators for aqueous processes in the Columbia Hills of Gusev Crater, Mars. *Journal of Geophysical Research*, 111, E02S12. <https://doi.org/10.1029/2005je002560>
- Montarges-Pelletier, E., Bogenez, S., Pelletier, M., Razafitianamaharavo, A., Ghanbaja, J., Lartiges, B., et al. (2005). Synthetic allophane-like particles: Textural properties. *Colloids and Surfaces A: Physicochemical and Engineering Aspects*, 255(1), 1–10. <https://doi.org/10.1016/j.colsurfa.2004.11.036>
- Murad, E. (1979). Mössbauer and X-ray data on  $\beta$ -FeOOH (akaganeite). *Clay Minerals*, 14(4), 273–283. <https://doi.org/10.1180/claymin.1979.014.4.04>
- Murad, E. (1987). Mössbauer spectra of nontronites: Structural implications and characterization of associated iron oxides. *Zeitschrift Fur Pflanzenernahrung Und Bodenkunde*, 150(5), 279–285. <https://doi.org/10.1002/jpln.19871500503>
- Murad, E., & Bishop, J. L. (2000). The infrared spectrum of synthetic akaganeite, beta-FeOOH. *American Mineralogist*, 85(5–6), 716–721. <https://doi.org/10.2138/am-2000-5-609>
- Naren, G., Ohashi, H., Okaue, Y., & Yokoyama, T. (2013). Adsorption kinetics of silicic acid on Akaganeite. *Journal of Colloid and Interface Science*, 399, 87–91. <https://doi.org/10.1016/j.jcis.2013.02.032>
- Ossaka, J., Iwai, S., Kasai, M., Shirai, T., & Hamada, S. (1971). Coexistence states of iron in synthesized iron-bearing allophane ( $\text{Al}_2\text{O}_3$ - $\text{SiO}_2$ - $\text{Fe}_2\text{O}_3$ - $\text{H}_2\text{O}$  system). *Bulletin of the Chemical Society of Japan*, 44(3), 716–718. <https://doi.org/10.1246/bcsj.44.716>
- Parfitt, R. L. (1990). Allophane in New Zealand - A review. *Australian Journal of Soil Research*, 28(3), 343–360. <https://doi.org/10.1071/Sr9900343>
- Parfitt, R. L., Childs, C. W., & Eden, D. N. (1988). Ferrihydrite and allophane in four Andepts from Hawaii and implications for their classification. *Geoderma*, 41(3), 223–241. [https://doi.org/10.1016/0016-7061\(88\)90062-6](https://doi.org/10.1016/0016-7061(88)90062-6)
- Peretyazhko, T. S., Pan, M. J., Ming, D. W., Rampe, E. B., Morris, R. V., & Agresti, D. G. (2019). Reaction of akaganeite with Mars-relevant anions. *ACS Earth and Space Chemistry*, 3(2), 314–323. <https://doi.org/10.1021/acsearthspacechem.8b00173>
- Post, J. E., Heaney, P. J., Von Dreele, R. B., & Hanson, J. C. (2003). Neutron and temperature-resolved synchrotron X-ray powder diffraction study of akaganeite. *American Mineralogist*, 88(5–6), 782–788. <https://doi.org/10.2138/am-2003-5-607>
- Poulet, F., Bibring, J. P., Mustard, J. F., Gendrin, A., Mangold, N., Langevin, Y., et al. (2005). Phyllosilicates on Mars and implications for early martian climate. *Nature*, 438(7068), 623–627. <https://doi.org/10.1038/nature04274>
- Rampe, E. B., Kraft, M. D., Sharp, T. G., Golden, D. C., Ming, D. W., & Christensen, P. R. (2012). Allophane detection on Mars with thermal emission spectrometer data and implications for regional-scale chemical weathering processes. *Geology*, 40(11), 995–998. <https://doi.org/10.1130/g33215.1>
- Rampe, E. B., Bristow, T. F., Morris, R. V., Morrison, S. M., Achilles, C. N., Ming, D. W., et al. (2020). Mineralogy of Vera Rubin Ridge from the Mars Science Laboratory CheMin Instrument. *Journal of Geophysical Research: Planets*, 125(9), e2019JE006306. <https://doi.org/10.1029/2019JE006306>
- Réguer, S., Dillmann, P., & Mirambet, F. (2007). Buried iron archaeological artefacts: Corrosion mechanisms related to the presence of Cl-containing phases. *Corrosion Science*, 49(6), 2726–2744. <https://doi.org/10.1016/j.corsci.2006.11.009>
- Rezel, D., & Genin, J. M. R. (1990). The substitution of chloride ions to  $\text{OH}^-$  ions in the akaganeite beta ferric oxyhydroxide studied by Mössbauer effect. *Hyperfine Interactions*, 57(1), 2067–2075. <https://doi.org/10.1007/bf02405765>
- Schwertmann, U., & Cornell, R. M. (1991). *Iron oxides in the laboratory: Preparation and characterization*. New York, NY: VCH.
- Schwertmann, U., & Thalmann, H. (1976). The influence of  $[\text{Fe}(\text{II})]$ ,  $[\text{Si}]$ , and pH on the formation of lepidocrocite and ferrihydrite during oxidation of aqueous  $\text{FeCl}_2$  solutions. *Clay Minerals*, 11(3), 189–200. <https://doi.org/10.1180/claymin.1976.011.3.02>
- Silva-Yumi, J., Escudey, M., Gacitua, M., & Pizarro, C. (2018). Kinetics, adsorption and desorption of Cd (II) and Cu (II) on natural allophane: Effect of iron oxide coating. *Geoderma*, 319, 70–79. <https://doi.org/10.1016/j.geoderma.2017.12.038>
- Ståhl, K., Nielsen, K., Jiang, J., Lebeck, B., Hanson, J. C., Norby, P., et al. (2003). On the akaganeite crystal structure, phase transformations and possible role in post-excavational corrosion of iron artifacts. *Corrosion Science*, 45(11), 2563–2575. [https://doi.org/10.1016/S0010-938X\(03\)00078-7](https://doi.org/10.1016/S0010-938X(03)00078-7)

- Sugimoto, T., Itoh, H., & Mochida, T. (1998). Shape control of monodisperse hematite particles by organic additives in the gel-sol system. *Journal of Colloid and Interface Science*, *205*(1), 42–52. <https://doi.org/10.1006/jcis.1998.5588>
- Sun, X., Hu, C., Hu, X., Qu, J., & Yang, M. (2013). Characterization and adsorption performance of Zr-doped akaganeite for efficient arsenic removal. *Journal of Chemical Technology and Biotechnology*, *88*(4), 629–635. <https://doi.org/10.1002/jctb.3878>
- Tamrat, W. Z., Rose, J., Grauby, O., Doelsch, E., Levard, C., Chaurand, P., et al. (2019). Soil organo-mineral associations formed by co-precipitation of Fe, Si and Al in presence of organic ligands. *Geochimica et Cosmochimica Acta*, *260*, 15–28. <https://doi.org/10.1016/j.gca.2019.05.043>
- Vaniman, D. T., Bish, D. L., Ming, D. W., Bristow, T. F., Morris, R. V., Blake, D. F., et al. (2014). Mineralogy of a mudstone at Yellowknife Bay, Gale crater, Mars. *Science*, *343*(6169), 1243480. <https://doi.org/10.1126/science.1243480>
- Viviano-Beck, C. E., Seelos, F. P., Murchie, S. L., Kahn, E. G., Seelos, K. D., Taylor, H. W., et al. (2014). Revised CRISM spectral parameters and summary products based on the currently detected mineral diversity on Mars. *Journal of Geophysical Research: Planets*, *119*(6), 1403–1431. <https://doi.org/10.1002/2014je004627>
- Wada, K. (1987). Minerals formed and mineral formation from volcanic ash by weathering. *Chemical Geology*, *60*(1), 17–28. [https://doi.org/10.1016/0009-2541\(87\)90106-9](https://doi.org/10.1016/0009-2541(87)90106-9)
- Wada, K. (1989). Allophane and imogolite. In J. B. Dixon, & S. B. Weed (Eds.), *Minerals in soil environments* (pp. 1051–1087). Madison, WI: Soil Science Society of America.
- Wang, S., Du, P., Yuan, P., Zhong, X., Liu, Y., Liu, D., et al. (2018). Changes in the structure and porosity of hollow spherical allophane under alkaline conditions. *Applied Clay Science*, *166*, 242–249. <https://doi.org/10.1016/j.clay.2018.09.028>
- Weitz, C. M., Bishop, J. L., Baker, L. L., & Berman, D. C. (2014). Fresh exposures of hydrous Fe-bearing amorphous silicates on Mars. *Geophysical Research Letters*, *41*(24), 8744–8751. <https://doi.org/10.1002/2014GL062065>
- Wilson, J., Cressey, G., Cressey, B., Cuadros, J., Ragnarsdottir, K. V., Savage, D., et al. (2006). The effect of iron on montmorillonite stability. (II) Experimental investigation. *Geochimica et Cosmochimica Acta*, *70*(2), 323–336. <https://doi.org/10.1016/j.gca.2005.09.023>